Desalination and Water Treatment
www.deswater.com
doi: 10.1080/19443994.2015.1017743

57 (2016) 8526–8539
April

Taylor & Francis
Taylor & Francis Group

Adsorption of Ni(II) using amine-functionalized MCM-41 optimized by response surface methodology

Shengxin Yang[a], Yunhai Wu[b,*], Ayinigaer Aierken[a], Meili Zhang[a], Yunying Wu[c]

[a]*College of Environment, Hohai University, Xikang Road #1, Nanjing 210098, China, emails: yangshengxin1234@163.com (S. Yang), hjyshiz@126.com (A. Aierken), hjyshiz@sohu.com (M. Zhang)*
[b]*Key Laboratory of Integrated Regulation and Resources Development of Shallow Lakes, Ministry of Education, Hohai University, Xikang Road #1, Nanjing 210098, China, Tel./Fax: +86 25 83786697; email: ysxhohai@163.com*
[c]*Department of Chemistry, Hanshan Normal University, Chaozhou, Guangdong province, China, email: ysxhohai@sina.cn*

Received 1 August 2014; Accepted 4 February 2015

ABSTRACT

Adsorption of Ni(II) by amine-functionalized MCM-41 (NH_2-MCM-41) was studied with response surface methodology (RSM) employed to optimize the adsorption process. The independent variables include pH, metal concentration, temperature, and adsorbent dosage. Analysis of variance (ANOVA) of RSM indicated that the obtained second-order polynomial model was appropriate to predict the adsorption process. Meanwhile, the maximum removal efficiency for Ni(II) was 93.20%, which was achieved at pH 6.50, metal concentration 10.00 mg/L, temperature 35°C, and adsorbent dosage 5.00 g/L. The kinetic study revealed that the pseudo-second-order kinetic model could describe the experimental data better. While the intraparticle diffusion model suggested three stages of the adsorption process. In addition, the adsorption data conformed well to Langmuir isotherm model. Thermodynamic study implied the adsorption process was spontaneous and endothermic. The adsorption–desorption experiment showed that NH_2-MCM-41 held good reusability.

Keywords: Ni(II); NH_2-MCM-41; Response surface methodology; Kinetic; Isotherm

1. Introduction

The immoderate discharge of wastewater-containing heavy metals can pollute the surface and ground water, which may threaten the fresh water sources, and then be hazardous to animals and human beings. Among the various heavy metal ions, nickel is known as one of the toxic elements. Excess uptake of nickel (estimated as 0.05 mg/cm^3 in nickel per 40 h work [1]) may directly or indirectly cause health effects on human beings, for example, diarrhoea, nephritic syndrome, serious lung and kidney problems, pulmonary fibrosis, and skin dermatitis [2]. In view of this, the World Health Organization has set the permissible limit of 0.02 mg/L for nickel in drinking water. However, wastewater discharge from industries, such as batteries manufacturing, mine, electronic, electroplating, and metal cleaning [3] often contains high concentrations of nickel that may cause serious problems. Thus, it is essential to removal nickel from wastewater before its emission.

As one of the most effective and attractive method, adsorption, with the advantages of no chemical sludge and high removal efficiency [4,5], has been widely

*Corresponding author.

used in the removal of heavy metal ion from aqueous solution. Furthermore, researcher has made enormous effort in the exploitation of new, cheaper, and effective adsorbents for heavy metal removal in the recent years. The tested adsorbents include zeolites [6], natural kaolinite [7], activated carbon prepared from apricot stone [8], tea factory waste [9], rice bran [10], and so on. In the family of mesoporous materials, MCM-41 plays a significant role. It owns large pore volume, high surface area, regular channel, and good thermostability [11,12], which made it a potential adsorbent. Hokura et al. [13] reported the adsorption of Cu(II) by MCM-41 and they found it effective as an adsorbent; Parida and Dash [14] reported that adsorption capacity of Fe-MCM-41 toward Cu(II) reached maximum at pH 5.5, temperature 323 K, and Cu(II) concentration of 59.6 mg/L; Qin et al. [15] demonstrated ammonium-functionalized MCM-41 was effective in absorbing four kinds of anionic dyes. Moreover, MCM-41 was usually modified to achieve better adsorption results.

Response surface methodology (RSM) is one of the most popularly used methods in research on sorption [16]. It combines mathematical and statistical techniques to evaluate the relative significance of process parameters in the presence of complex interactions [17], as well as to capture the nonlinear relationships between independent parameters and system response.

In the present work, amine-functionalized MCM-41 was synthesized and used as an adsorbent in the removal of Ni(II) from solution. Moreover, RSM was employed to optimize the adsorption process with variables such as pH, metal concentration, temperature, and adsorbent dosage studied. Adsorption isotherms were applied to describe the equilibrium data. Kinetics and thermodynamics were also studied for better evaluating the adsorption mechanism. At last, regeneration of the adsorbent was tested as well. The aim of this paper is to show the availability of NH_2-MCM-41 to adsorb Ni(II) from solution.

2. Materials and methods

2.1. Materials

A stock solution of Ni(II) (1,000 mg/L) was prepared in the way as follows: 0.1000 g Ni (99.9%) dissolved in 10 mL of (1 + 1) Nitric Acid, then the solution was heated to nearly dry, followed by dissolving the solid in 1% Nitric Acid, and then diluted with distilled water to 1,000 mL. The stock solution was diluted with distilled water to obtain desired concentration in experiments.

2.2. Characterization of the adsorbent

The pristine MCM-41 was purchased (Tianjin kay, science and technology development co., Ltd., China) and NH_2-MCM-41 was synthesized according to the method in our previous work [18]. All other chemicals used were of analytical grade and used without further purification. Nitrogen adsorption–desorption isotherms were determined by an ASAP 2010. X-ray diffraction (XRD) of the adsorbent was measured with an X-ray diffractometer (ARL Corporation, Switzerland) using Ni filter CuKα at 40 kV and 30 mA over the range of 1°–8°. Besides, in order to analyze the chemical properties of NH_2-MCM-41 before and after adsorption, Fourier transform infrared (FTIR) spectra was obtained using a Bruker corporation instrument (German) with all spectra recorded at 4,000–750 cm^{-1} wavenumber. Moreover, microscopic appearance of the adsorbent was studied by field emission scanning electron microscope (SEM) (S4800, Carl Zeiss AG, Germany) with the images taken at 5.0 kV. X-ray Fluorescence (XRF) (Thermofisher Scientific Corporation) was used to analyze the adsorbent chemical composites.

The pH in the point of zero charge (pH_{pzc}) for NH_2-MCM-41 was determined as follows [19]: 25 mL of 0.01 M NaCl were added to a series of 250 mL conical flasks, and the initial pH was adjusted between 2 and 12 using 0.1 M NaOH or 0.1 M HCl. Then, 0.08 g of NH_2-MCM-41 was added to each flask with the final pH measured after agitation for 48 h. Afterward, difference between the initial pH and final pH (initial pH–final pH) was plotted against the initial pH. The point, at which the resulting curve intersected with abscissa, gave the pH_{pzc}.

2.3. Adsorption studies

Batch adsorption experiments were conducted according to the RSM design. The experiments were carried out in conical flasks of 250 mL containing 100 mL nickel solution at a known concentration. pH of the solution was adjusted with 0.1 M HCl or NaOH. Then, the conical flasks were placed in a shaker at 130 rpm for 180 min. After adsorption, the samples were separated by centrifugation at 8,000 rpm, and the supernatant was used to determine the residual nickel concentration with a UV-spectrophotometer (Ruili Analytical Instrument Corporation Ltd., Beijing, China) at 530 nm. In addition, the comparison experiment was conducted with 0.1 g MCM-41 and NH_2-MCM-41 respective with 100 mL of metal solution (10 mg/L) at pH 6.0. For isotherm study, experiments

were carried out with 0.35 g adsorbent, metal concentration in the range of 10–50 mg/L, at pH 6.5, and temperature 25, 30, and 40˚C, respectively. For kinetic study, experiments were performed with 0.35 g of NH_2-MCM-41, 100 mL of nickel solution (30 mg/L) at 30˚C, and pH 6.5. And the supernatant was withdrawn at 15, 30, 60, 90, 120, 150, and 180 min, separately. The Removal (%) and adsorption capacity q_e (mg/g) were calculated by the equations following:

$$\text{Removal} = \frac{C_0 - C_e}{C_0} \times 100\% \quad (1)$$

$$q_e = \frac{(C_0 - C_e)V}{M} \quad (2)$$

where C_0 is the initial Ni(II) concentration (mg/L), C_e is the final Ni(II) concentration (mg/L), V(mL) is the volume of solution, and M(g) is the mass of dry adsorbent. All these experiments were conducted in triplicate.

2.4. Desorption study

After adsorption process, the adsorbent was recovered by mixing metal-loaded adsorbent with 25 mL of 1 M HNO_3, and agitated at the speed of 130 rpm for 180 min.

2.5. Experimental design

The Design Expert software (Stat-Ease, Inc., Minneapolis, USA) was used for regression and graphical analysis of the experimental data.

The optimum conditions for the adsorption of Ni(II) by NH_2-MCM-41 was determined based on a central composite design (CCD) under RSM. And the optimum studies were carried out with four response variables: pH (X_1), metal concentration (X_2), temperature (X_3), and adsorbent dosage (X_4). For statistical calculation, the variables X_i were coded as Z_i according to the following equation:

$$Z_i = \frac{X_i - X_0}{\Delta X} \quad (3)$$

where Z_i is a coded value of the variable, X_i is actual value of variable, X_0 is value of the X_i at the center point, and ΔX the step change value. The actual value and coded value of the variables are shown in Table 1. To explain relationship between the independent variables and the response, a quadratic equation was used:

$$R\ (\%) = a_0 + \sum_{i=1}^{n} a_i X_i + \sum_{i=1}^{n} a_{ii} X_i^2 + \sum_{i=1}^{n-1} \sum_{j=2}^{n} a_{ij} X_i X_j + e \quad (4)$$

where a_0 is the constant coefficient, a_i, a_{ii}, and a_{ij} are the regression coefficients, X_i and X_j indicate the independent variables in the form of coded values, and e is the random error.

3. Results and discussion

3.1. Characterization of the adsorbent

The BET surface area, total pore volume, and mean pore radius of NH_2-MCM-41 were 658 m^2/g, 0.78 cm^3/g, and 2.74 nm, respectively, while that of MCM-41 were 821 m^2/g, 0.94 cm^3/g, and 3.02 nm, respectively. There existed significant decrease in the surface area, total pore volume, and mean pore radius of NH_2-MCM-41 when compared with MCM-41. This may result from the amine groups in the framework channels [20] and adsorbent surface.

The XRD spectra of MCM-41, NH_2-MCM-41, NH_2-MCM-41-Ni, and Ni-desorbed NH_2-MCM-41 in the range of 1˚–8˚ were illustrated in Fig. 1. As shown in Fig. 1, all spectra owned a diffraction peak in the range of 1˚–3˚, even though the intensity of the peak decreased, corresponding to the (100) plane of hexagonal cell of MCM-41. The intensity decrease of the (100) plane and the disappearance of the (110) plane may due to the graft of amine. Thus, it can be confirmed that the hexagonal structure of MCM-41 was preserved after modified by amine group. In addition, the XRD patterns of NH_2-MCM-41 before and after the regeneration had the similar trend, demonstrating that the effect of adsorbent regeneration process on the structure of NH_2-MCM-41 was weak.

FTIR spectrum of NH_2-MCM-41 before and after adsorption of Ni(II) are shown in Fig. 2. The FTIR analysis had shown that amino was successfully grafted on MCM-41 in our previous work [18]. Upon Ni(II) loading, the peak intensity of NH_2-MCM-41 at 1,541.1/cm (bending vibration of N–H group) was weakened, this may be attributed to the presence of a lesser number of functional groups on NH_2-MCM-41 [21]. Moreover, the peak at 1,541.1/cm exhibited band shift. Thus, we speculated it was caused by the adsorption of Ni(II), and the amine group may be involved in the adsorption process. This point was also reported by other researchers (Malkoc and Nuhoglu [3], Sheng et al. [22]). Besides, Sun et al. [23] studied the adsorption of heavy metal

Table 1
The independent variables and their levels in the experiment design

Factors		Coded values				
		−α (−2)	−1	0	1	α (2)
pH	X_1	0.5	2.5	5	7.5	10
Metal concentration (mg/L)	X_2	0	10	30	50	70
Temperature (ºC)	X_3	10	20	30	40	50
Adsorbent dosage (g/L)	X_4	0	1	3	5	7

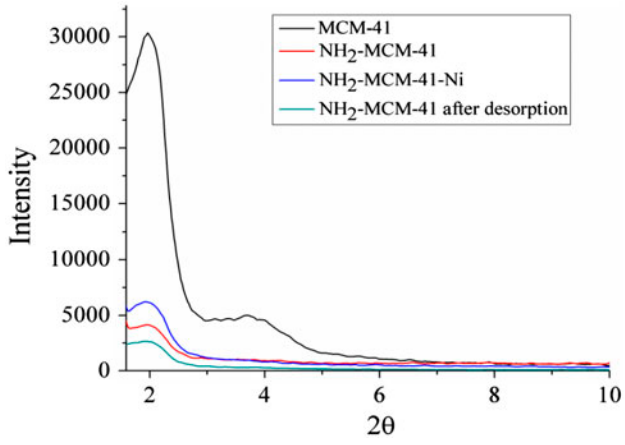

Fig. 1. Small angle XRD spectra of MCM-41, NH_2-MCM-41, NH_2-MCM-41-Ni, and desorbed NH_2-MCM-41.

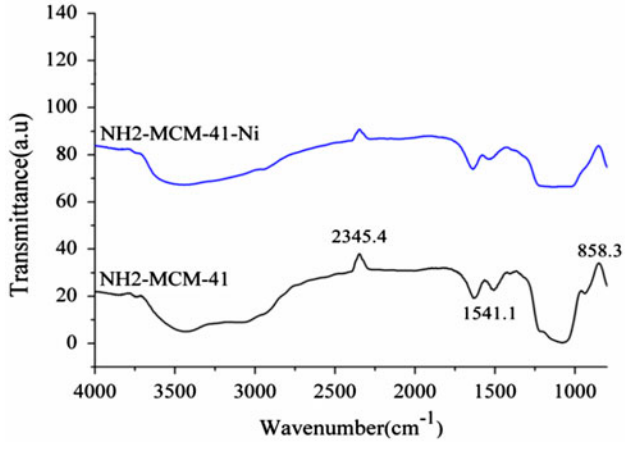

Fig. 2. FTIR spectra of NH_2-MCM-41 and NH_2-MCM-41-Ni.

ions on chitosan/cellulose composite biosorbent. The 1,599/cm (–NH bending vibration) was weakened after adsorption and they inferred that the amine group was involved in the adsorption process. Moreover, Ni(II)–N coordinate bonds were claimed to be formed. Boddu et al. [21] reported the removal of arsenic(III) and (V) using chitosan-coated biosorbent. In their study, the intensity of transmittance of peaks (–NH vibration) was relatively more in case of metal ions-loaded adsorbent, and they attributed this to the lesser number of functional groups (including $–NH_2$) that involved in binding the metal ions.

The FE-SEM images of MCM-41, NH_2-MCM-41, and Ni-loaded NH_2-MCM-41 were provided as shown in Fig. 3. Compared with MCM-41, the image of NH_2-MCM-41 showed that the graft of amine groups on MCM-41 did not bring about significant change to the mesoporous structure of MCM-41. While some of the pore may be blocked. Whereas, a large number of tiny particles emerged on the surface of NH_2-MCM-41 after Ni(II) adsorption process as illustrated in Fig. 3(c); it may imply that Ni(II) could be successfully adsorbed on NH_2-MCM-41.

3.2. Comparison removal efficiency

A comparison for the removal efficiency of Ni(II) by NH_2-MCM-41 and MCM-41 was made, as shown in Fig. 4. It can be seen from Fig. 4 that the Ni(II) removal efficiency were, respectively, 70.51 and 39.42% for NH_2-MCM-41 and MCM-41. The grafted of amidogen on MCM-41 had greatly improved the adsorption capacity of MCM-41 for Ni(II). Therefore, NH_2-MCM-41 owned the potential to be used in the removal of Ni(II).

3.3. Fitting of the process model and statistical analysis

In the optimization experiment, a total of 30 runs of CCD-designed experiments were conducted and the results are presented in Table 2. Through multiple regression analysis on the experiment data, the predicted model, a second-order polynomial function, was achieved:

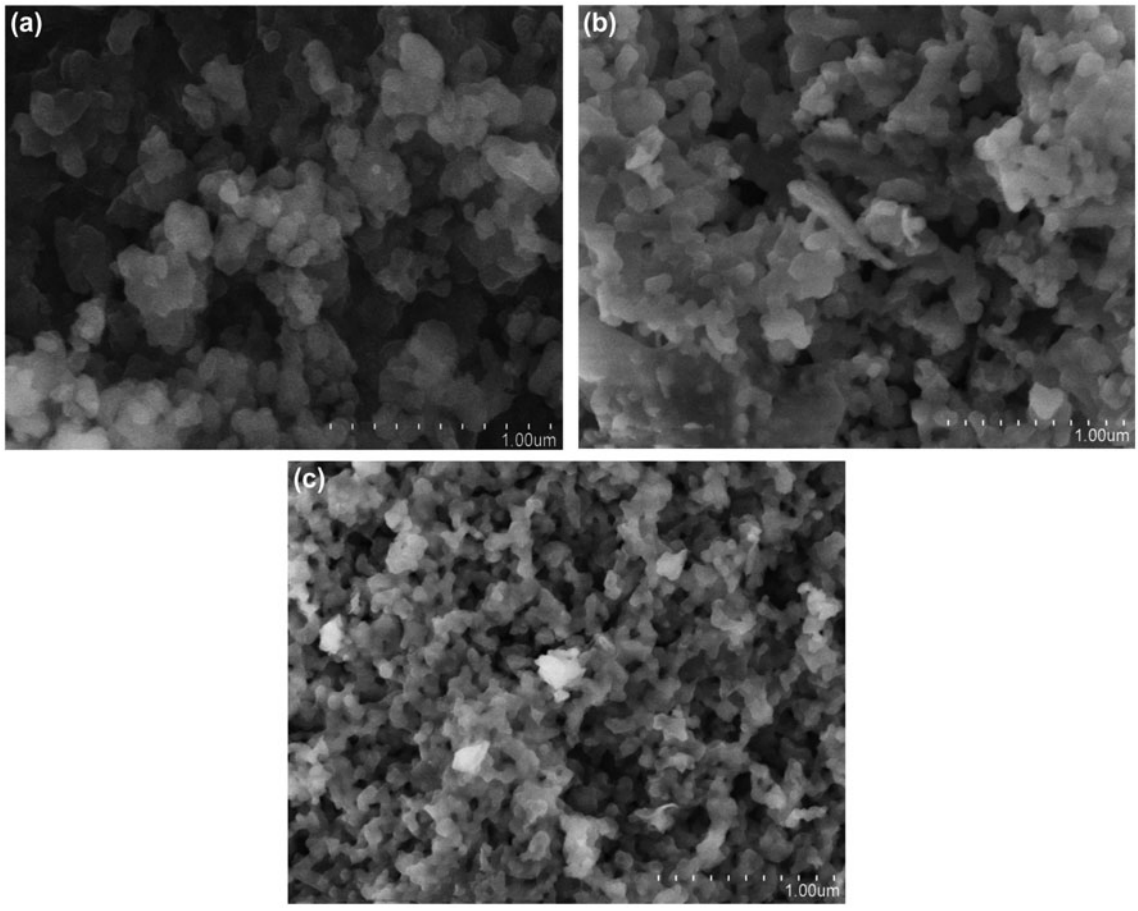

Fig. 3. SEM images of MCM-41 (a), NH_2-MCM-41 (b), and Ni-loaded NH_2-MCM-41 (c).

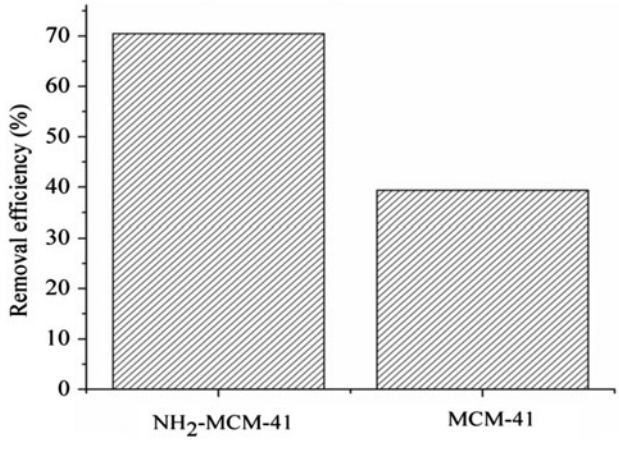

Fig. 4. Comparison removal efficiency of NH_2-MCM-41 and MCM-41 for Ni(II).

$$Y_{\mathrm{Ni(II)}} = 48.50 + 15.22X_1 - 12.45X_2 + 8.50X_3 + 10.76X_4 + 4.16X_1^2 + 6.49X_2^2 - 3.86X_3^2 - 4.26X_4^2 - 1.81X_1X_3 + 2.72X_1X_4 + 3.04X_2X_3 \quad (5)$$

In this equation, the positive values indicated that these terms increase the response, while the negative values decrease the response [24]. The results of Analysis of variance (ANOVA) for the predicted model and each variable are given in Table 3. In Table 3, the large model F value (73.35) and low probability "p" value (<0.0001) indicated high significance of the predicted model. It implied that the model can explain relation between the response and variables appropriately. Moreover, applicability of the model can be checked by the determined coefficient (R^2) and adjusted R^2_{adj} [25] as well. The value of R^2 (0.9856) and adjusted R^2_{adj} (0.9722) were all close to 1, which demonstrated applicability of the model as well as a high correlation between the actual and predicted values.

Table 2
Experiment design and results of the CCD

Run order	Coded values				Response (%)	
	X_1	X_2	X_3	X_4	Observed value	Predicted value
1	−1	−1	−1	−1	37.50	35.73
2	+1	−1	−1	−1	63.50	62.68
3	−1	1	−1	−1	6.80	1.26
4	1	1	−1	−1	31.20	29.88
5	−1	−1	1	−1	52.50	49.45
6	1	−1	1	−1	70.70	69.17
7	−1	1	1	−1	29.20	27.15
8	1	1	1	−1	50.80	48.55
9	−1	−1	−1	1	48.90	47.76
10	1	−1	−1	1	85.10	86.22
11	−1	1	−1	1	18.60	19.20
12	1	1	−1	1	58.40	58.70
13	−1	−1	1	1	63.30	63.38
14	1	−1	1	1	91.50	94.28
15	−1	1	1	1	48.60	46.66
16	1	1	1	1	78.10	78.93
17	−2	0	0	0	32.50	37.59
18	2	0	0	0	98.20	96.80
19	0	−2	0	0	99.10	98.95
20	0	2	0	0	45.30	49.14
21	0	0	−2	0	13.60	15.72
22	0	0	2	0	48.10	49.67
23	0	0	0	−2	2.20	9.52
24	0	0	0	2	56.20	52.57
25	0	0	0	0	48.40	48.38
26	0	0	0	0	48.50	48.38
27	0	0	0	0	48.10	48.38
28	0	0	0	0	48.30	48.38
29	0	0	0	0	48.60	48.38
30	0	0	0	0	48.40	48.38

Besides, the predicted vs. actual removal efficiency for Ni(II) are illustrated in Fig. 5, where the predicted values were calculated according to Eq. (5) and the actual values were measured data for each run in the CCD design. It can be detected from Fig. 5 that the predicted and actual values were in good agreement.

3.4. Effect of process variables

Sensitivity of the response to two interactive variables can be displayed by holding the other variables at central values. Based on the ANOVA results, the pH with a *F*-value of 334.23 and "*p*" value less than 0.0001 was found to have the greatest effect on the removal of Ni(II) by NH_2-MCM-41. The other three variables also exhibited significant effect on Ni(II) removal in the order of metal concentration ($F = 223.77$, $p < 0.0001$) > adsorbent dosage ($F = 167.11$, $p < 0.0001$) > temperature ($F = 104.13$, $p < 0.0001$). The effect of the four process variables on the response are shown in the 3D response surface plots (Figs. 6(a)–(c) and 7(a)–(c)).

3.4.1. Effect of pH

The combined effects of pH with metal concentration, temperature, and adsorbent dosage are shown in Fig. 6(a)–(c). As can be seen from Fig. 6(a)–(c), the removal efficiency of Ni(II) increased with increase pH ranging from 2.5 to 6.5. This phenomenon can be explained by the different dominant form of Ni(II). It is clear that Ni(II) presents in the forms of Ni^{2+}, $Ni(OH)^+$, $Ni(OH)^0_2$, and $Ni(OH)^-_3$ at different pH values (Fig. 8(a)). At pH < 8.0, the main species is Ni^{2+}.

Table 3
ANOVA for the fitted quadratic polynomial model for Ni(II) adsorption

Source	Sum of squares	df	Mean square	*F*-value	*Prob* > *F*
Model	16,935.24	14	1,209.66	96.58	<0.0001
X_1	5,259.92	1	5,259.92	419.94	<0.0001
X_2	3,722.55	1	3,722.55	297.20	<0.0001
X_3	1,728.90	1	1,728.90	138.03	<0.0001
X_4	2,779.95	1	2,779.95	221.95	<0.0001
X_1X_2	2.81	1	2.81	0.22	0.6428
X_1X_3	52.20	1	52.20	4.17	0.0592
X_1X_4	118.27	1	118.27	9.44	0.0077
X_2X_3	148.23	1	148.23	11.83	0.0036
X_2X_4	27.83	1	27.83	2.22	0.1568
X_3X_4	2.48	1	2.48	0.20	0.6627
X_1^2	606.70	1	606.70	48.44	<0.0001
X_2^2	1,128.97	1	1,128.97	90.13	<0.0001
X_3^2	421.88	1	421.88	33.68	<0.0001
X_4^2	515.30	1	515.30	41.14	<0.0001
Residual	187.88	15	12.53		
Lack of fit	187.33	10	18.77	632.81	<0.0001
Pure error	0.15	5	0.030		
Cor total	17,123.12	29			

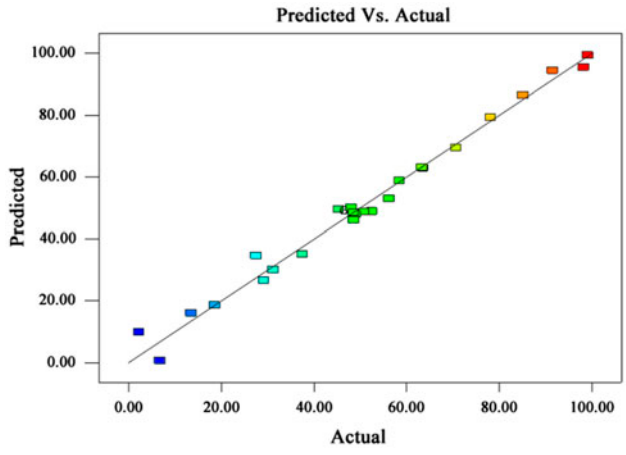

Fig. 5. Correlation of actual and predicted removal efficiency for Ni(II).

Thus, the low Ni(II) removal efficiency under initial strong acidic condition may be attributed to the competition between H^+ and Ni^{2+} for active adsorption sites. Besides, the pH_{pzc} of NH_2-MCM-41 was about 9.72 (Fig. 8(b)), then NH_2-MCM-41 would be protonated and positively charged under pH 9.72, so the repulsive force between the positively charged NH_2-MCM-41 and Ni^{2+} may also inhibit the adsorption of Ni(II). However, when pH increased, some of the adsorption sites would be released and the adsorbent surface could also be deprotonated to some extent, promoting the adsorption of Ni(II) and increasing the removal efficiency.

In addition, one can see from Fig. 6(a)–(c) that Ni(II) removal efficiency was more than 20% even at very low pH under any fixed metal concentration, temperature, and adsorbent dosage. As to this phenomenon, it can be speculated that cation exchange process between Ni^{2+} and the Al^{3+} on the adsorbent surface under acidic condition may also played a role in the removal of Ni(II) [26]. Moreover, at a higher pH, outer-sphere surface complexation maybe significant in the adsorption process [27]. Because a number of $–NH_2$ existed on the surface of NH_2-MCM-41, then Ni(II) would complex with $–NH_2$ on the adsorbent surface, which enhanced the removal of Ni(II). Sun et al. [23] reported that a lone pair of electrons in the nitrogen atom was donated to the shared bond between N and Ni(II) in the X-ray photoelectron spectroscopy analysis on the adsorption of Ni(II) by chitosan.

3.4.2. Effect of temperature

Figs. 6(b) and 7(a) and (c) illustrates the interaction effects of temperature with pH, metal concentration, and adsorbent dosage. It was obvious that Ni(II) removal efficiency increased gradually with increase in temperature, which indicated that high temperature was advantageous for Ni(II) removal. Besides, according to the linear coefficient (+8.50) of X_3 in Eq. (5), a

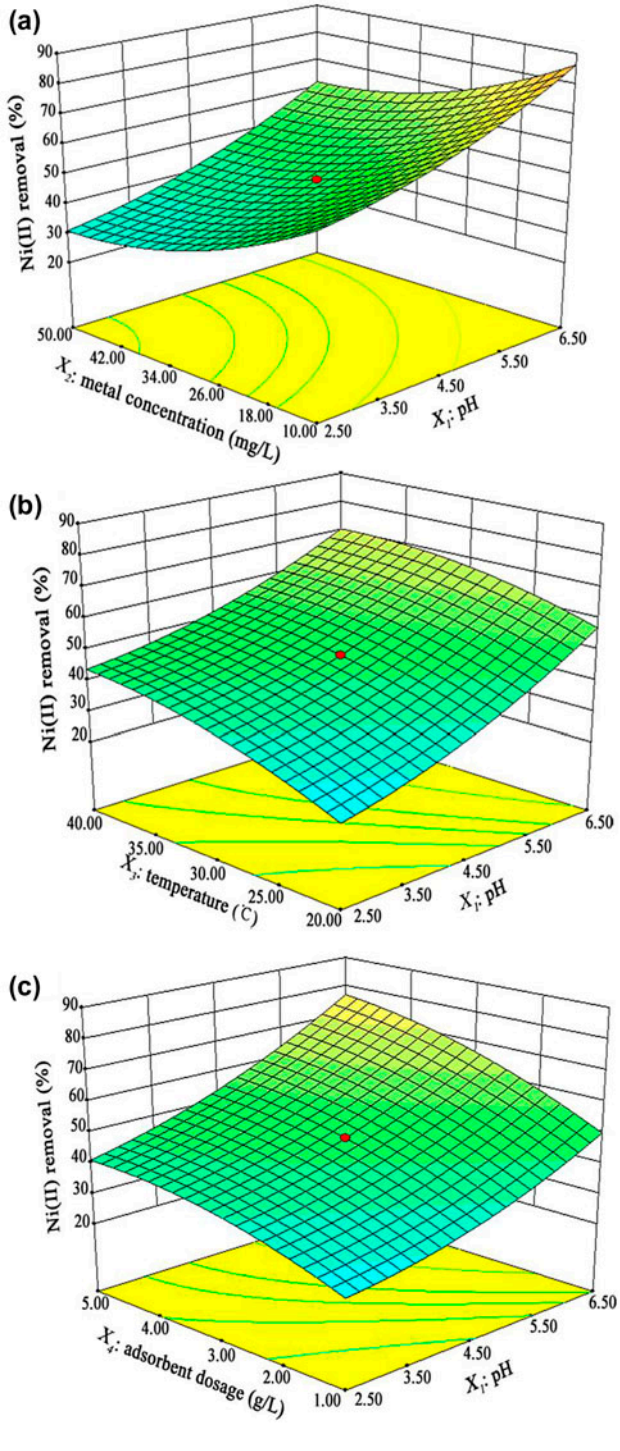

Fig. 6. Response surface plots for the combined effect of initial pH and metal concentration (a), initial pH and temperature (b), initial pH and adsorbent dosage (c) on the removal efficiency of Ni(II).

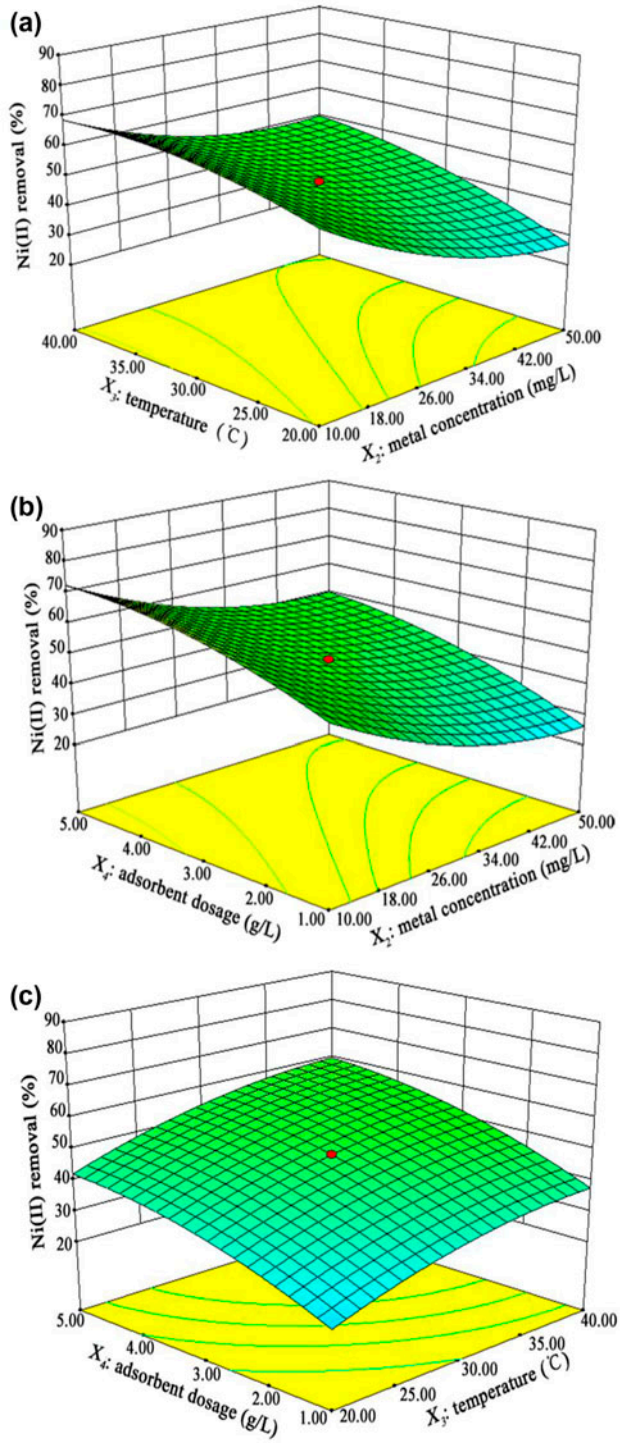

Fig. 7. Response surface plots for the combined effect of metal concentration and temperature (a), metal concentration and adsorbent dosage (b), temperature and adsorbent dosage (c) on the removal efficiency of Ni(II).

positive correlation between temperature and the removal efficiency of Ni(II) can be detected. On one hand, higher diffusion rate of Ni(II) across the external layer and into the adsorbent pores due to higher

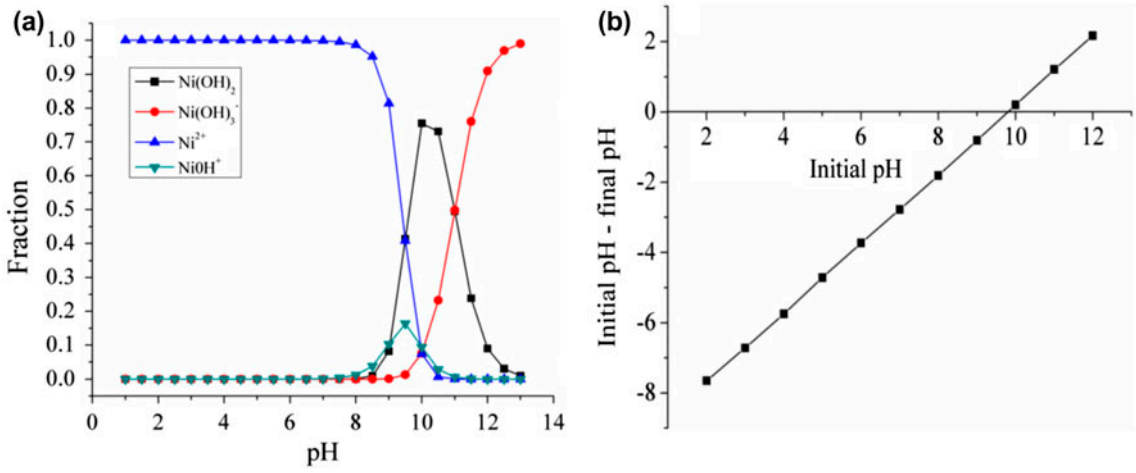

Fig. 8. (a) Diagram for Ni(II) chemical species in aqueous solution and (b) Point of zero charge.

temperature may account for the phenomenon [28]. On the other hand, because of the break of some bonds on adsorbent surface at higher temperature, more available active sites were released, thus enhanced the adsorption of Ni(II).

This situation can be interpreted through the thermodynamic parameters, for example, free energy (ΔG°), enthalpy (ΔH°), and entropy (ΔS°) as well. The ΔG°, ΔH°, and ΔS° were calculated from the following equations:

$$K_0 = \frac{C_{ad}}{C_e} \tag{6}$$

$$\Delta G = -RT \ln K_0 \tag{7}$$

$$\ln K_0 = \frac{\Delta S^\circ}{R} - \frac{\Delta H^\circ}{RT} \tag{8}$$

where K_0 is the equilibrium constant, C_{ad} is the amounts of metal ion on adsorbent phase (mg/L), R is the gas constant (8.314 J/K mol), and T is the temperature (K). ΔH° and ΔS° could be obtained from slope and intercept of the van't Hoff plot of ln k_0 vs. 1,000/T, respectively.

The thermodynamic parameters for adsorption of Ni(II) by NH_2-MCM-41 are summarized in Table 4. The negative values of ΔG° decreased with rise in temperature, implying the adsorption process was spontaneous and higher temperature promoted the adsorption of Ni(II). In addition, the positive value of ΔH° meant the adsorption process was endothermic and the positive ΔS° indicated affinity of the adsorbent towards Ni(II).

3.4.3. Effect of adsorbent dosage

The mutual effects of adsorbent dosage with pH, metal concentration, and temperature are visualized in Figs. 6(c) and 7(b) and (c). The results indicated that the removal percentage increased sharply with rise in adsorbent dosage from 1 to 3.5 g/L. While the increase of adsorbent dosage can hardly improve Ni(II) removal efficiency when it exceeded 3.5 g/L. With a fixed number of Ni(II) in the solution, the more the adsorbent dosage, the more the available adsorption sites were provided. However, when the adsorption process reached equilibrium, the residual Ni(II) in solution was little, and the driving force supplied by concentration gradient could not overcome the transfer resitance [29]. Moreover, there would be more chance of the adsorbent particles to collide with each other, which reduced the available adsorption sites in a certain degree.

3.4.4. Effect of metal concentration

As shown in Figs. 6(a) and 7(a) and (b), it can be ascertained that Ni(II) removal efficiency decreased with increasing metal concentration from 10 to 50 mg/L. When metal concentration was low, the adsorbent owned enough adsorption sites, so the removal efficiency was high. Whereas, the adsorption sites would become saturated at a high metal concentration, then the removal efficiency was low.

3.5. Confirmation experiments

To support suitability of the model for predicting the optimal condition: pH 6.50, metal concentration

Table 4
Thermodynamic parameters for the adsorption of Ni(II) by NH_2-MCM-41

Ion	Temperature(℃)	ΔG°(kJ/mol)	ΔH°(kJ/mol)	ΔS°(J/mol·K)
Ni(II)	25	−1.82	61.62	200.67
	30	−1.92		
	40	−2.04		

10.00 mg/L, temperature 35℃, and adsorbent dosage 5.00 g/L. Confirmation experiment was conducted under the optimal condition and the removal efficiency of Ni(II) reached 93.20%, which was in good agreement with the predicted 95.36% by RSM.

3.6. Adsorption isotherms

The study of adsorption isotherms is favorable to understand the relationship between adsorbent and adsorbate as well as provide more information about adsorption capacity of adsorbent. In the present work, the Langmuir, Freundlich, and Dubinin–Radushkevich (D–R) isotherm models were used to analyze the experiment data. The Langmuir model assumes a monolayer adsorption, insists the adsorption sites on adsorbent surface are identical, and there exists no interaction between the adsorbed molecules [30]:

$$q_e = \frac{q_m K_L C_e}{1 + K_L C_e} \tag{9}$$

where q_m (mg/g) is maximum adsorption capacity of the adsorbent, K_L (L/mg) presents the Langmuir adsorption constant. The Freundlich isotherm is usually used for assuming an uneven distribution of adsorption heat over the surface, and nonideal multilayer adsorption [31]:

$$q_e = K_F C_e^{1/n} \tag{10}$$

where K_F (mg/g) is a constant related to the relative sorption capacity of sorbent, n is a constant related to the intensity of sorption. The D–R model is mainly used to evaluate adsorption energy [32] and describe the sorption on both homogeneous and heterogeneous surfaces [33]:

$$q_e = q_m \exp(-K_{DR}\varepsilon^2) \tag{11}$$

$$\varepsilon = RT \ln\left(1 + \frac{1}{C_e}\right) \tag{12}$$

$$E = \frac{1}{\sqrt{2K_{DR}}} \tag{13}$$

where K_{DR} (mol^2/kJ^2) is the constant related to adsorption energy, ε is the polany potential, and E (kJ/mol) is the mean free energy of sorption. The adsorption is dominated by chemical ion exchange if E lies between 8 and 16 kJ/mol, whereas if E lower than 8 kJ/mol, the adsorption process is of a physical nature [34,35].

Fitted curves of the isotherm models and the corresponding parameters are shown in Fig. 9 and Table 5, respectively. Table 5 gave out the idea that Langmuir was better fitted to the experiment data for the higher R^2 values. Therefore, it can be concluded that the adsorption of Ni(II) may mainly happen on the surface of NH_2-MCM-41. Moreover, the maximum adsorption capacity was 14.34 mg/g. In comparison with the other adsorbent [1,36–41] as presented in Table 6, NH_2-MCM-41 had a good adsorption capacity and the potential to be employed in the removal of Ni(II) from solution. The E values obtained (10.976, 11.890, and 12.909 kJ/mol) were all in the range of 8–16 kJ/mol, indicating the adsorption of Ni(II) was chemical adsorption.

3.7. Kinetic study

For purpose of exploring the adsorption mechanism and having a deep insight into the adsorption process, both the pseudo-first-order [42] and pseudo-second-order [43] kinetic models have been used for fitting the experiment data. The linear form of pseudo-first-order (Eq. (14)) and pseudo-second-order (Eq. (15)) model are expressed as follows:

$$\ln\,(q_e - q_t) = \ln\, q_e - k_1 t \,/\, 2.303 \tag{14}$$

$$\frac{t}{q_t} = \frac{1}{k_2 q_e^2} + \frac{t}{q_e} \tag{15}$$

where q_t (mg/g) is the amount of metal ions adsorbed at time t, k_1 is the pseudo-first-order adsorption rate

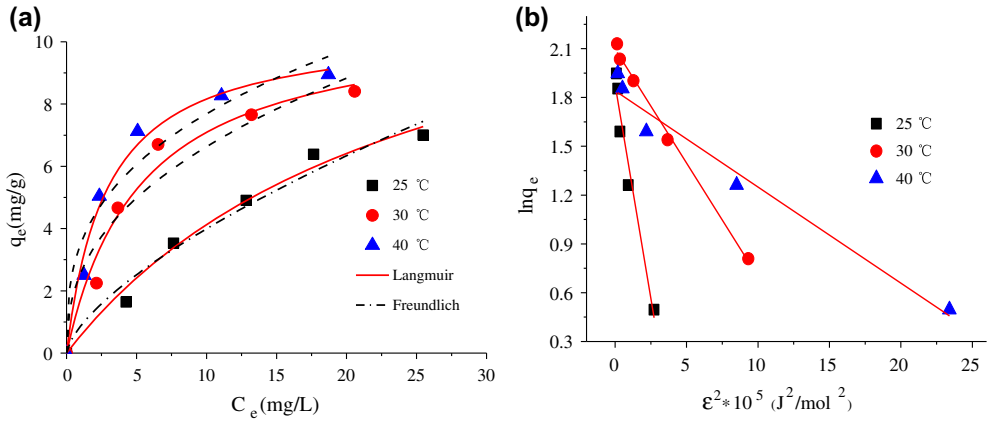

Fig. 9. The fitted curve of isotherm models at different temperature (a) Langmuir and Freundlich and (b) D–R.

Table 5
Isotherm parameters for the adsorption of Ni(II) by NH_2-MCM-41

		Langmuir			Freundlich			D–R			
Ion	Temperature (℃)	Q_0 (mg/g)	K_L	R^2	K_f	n	R^2	Q_m (mmol/g)	K (mol^2/kJ^2)	R^2	E (kJ/mol)
Ni(II)	25	14.34	0.040	0.984	0.862	1.501	0.968	6.546	0.525	0.952	10.98
	30	10.85	0.188	0.968	2.566	2.424	0.924	8.141	0.140	0.964	11.89
	40	10.51	0.347	0.984	3.489	2.915	0.934	6.301	0.059	0.964	12.91

Table 6
A comparison of adsorption of Ni(II) by different adsorbents

Adsorbent	Adsorption capacity (mg/g)	pH	Concentration (mg/L)	References
Lignocellulosic	2.76	5.8	150	[36]
Rice husk	11.50	6.5	200	[37]
Mixture grafted poly fiber	43.48	5.0	250	[38]
Leonardite	15.26	5.3	230.70	[39]
Brewery's yeast	5.34	6.0	100	[40]
Organic-inorganic silica composites	182	7.0	1,000	[1]
MCM-41	10.25	5.5	40	[41]
NH_2-MCM-41	14.34	6.5	50	This work

constant (per minute), and k_2 (g/(mg min)) is the pseudo-second-order adsorption rate constant.

The plots of log $(q_e - q_t)$ vs. t (Fig. 10 (a)) and t/q_t against t (Fig. 10 (b)) show the suitability of pseudo-first-order and pseudo-second-order kinetic models, respectively. And the related kinetic parameters are listed in Table 7. Comparing with pseudo-first-order kinetic model, pseudo-second-order described the experiment data better for a higher R^2 value. It meant that the rate-limiting step involved chemisorption [44].

Although the above two kinetic model revealed some information about the adsorption process, it could not provide more specific explaination. Therefore, the Spahn and Schlunder model and the intraparticle diffusion model were also employed in the present work. The Spahn and Schlunder model is usually used to describe the external diffusion process, in which the adsorbent across the film to the surface of adsorbent [45]. It can be expressed by the following equation:

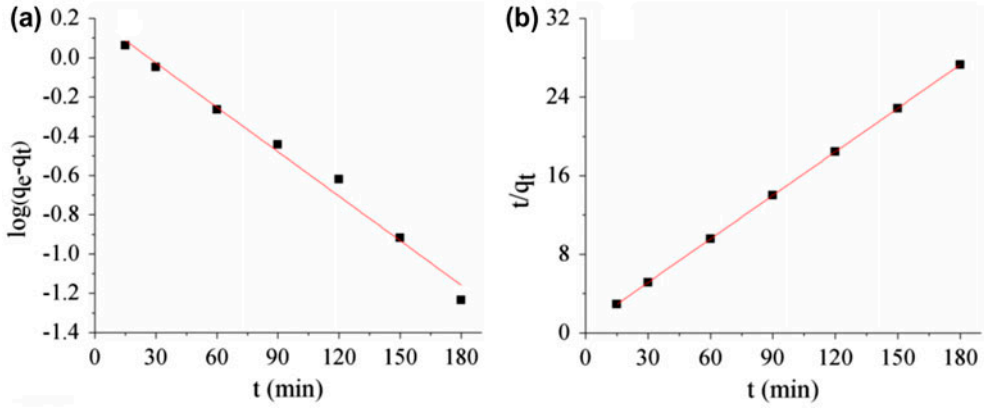

Fig. 10. Pseudo-first-order (a) and pseudo-second-order (b) for the adsorption of Ni(II) by NH_2-MCM-41.

Table 7
Kinetic parameters for the adsorption of Ni(II) by NH_2-MCM-41

	Pseudo-first-order kinetic			Pseudo-second-order kinetic			Intraparticle diffusion model	
Ion Ni(II)	k_1 (min^{-1})	q_e (mg/g)	R^2	k_2 (g/(mg min))	q_e (mg/g)	R^2	k_{2d} (mg/(g $min^{1/2}$))	k_{3d} (mg/(g $min^{1/2}$))
	0.0167	1.4802	0.9837	0.0306	6.7714	0.9995	0.1779	0.0464

$$\ln C_t = \ln C_0 - k_{ext}t \quad (16)$$

where C_t is the metal concentration at time t in mg/L, k_{ext} (1/min) is the external diffusion constant. If external diffusion rate is dominant in the whole adsorption process, ln C_t would exhibit a good linear relationship with t.

Fig. 11(a) shows the relationship of ln C_t with t. In Fig. 11(a), the ln C_t had a good linear shape in the initial 60 min, indicating external diffusion was primary in that period.

The intraparticle diffusion model is utilized to represent ion diffusion in the adsorbent micropore [46]:

$$q_t = k_{p,i}t^{0.5} \quad (17)$$

where $k_{p,i}$ is the intraparticle diffusion rate constant of different stages. In terms of this model, if the paragraph is consist of multilinear, then two or more steps are included in the adsorption process [47].

The paragraph of q_t vs. $t^{0.5}$ is presented in Fig. 11(b). As can be seen from Fig. 11(b), the paragraph emerged as three linear parts. The first part represented a extremely fast uptake, which was not shown in the figure. In this part, Ni(II) complexed with the active sites on adsorbent surface. The second part was by intraparticle diffusion, when the active adsorption sites on adsorbent surface were saturated, then Ni(II) diffused from surface into the micropore. During this period, the mass transfer resistance increased and the adsorption rate was slowed. The third part was the equilibrium stage because of the external or internal adsorption sites were all saturated, thereafter the adsorption process reached equilibrium.

3.8. XRF analysis

The chemical composition of NH_2-MCM-41 is analyzed by XRF and the data are shown in Table 8. The existence of nickel after adsorption was attributed to the complexation of nickel on the adsorbent surface.

3.9. Desorption and regeneration studies

In order to make NH_2-MCM-41 feasible and economical, adsorption–desorption studies were carried out. The result revealed that removal efficiency of Ni (II) decreased slightly along with the times used, and it can still be reached 84% after six times of adsorption–desorption experiments.

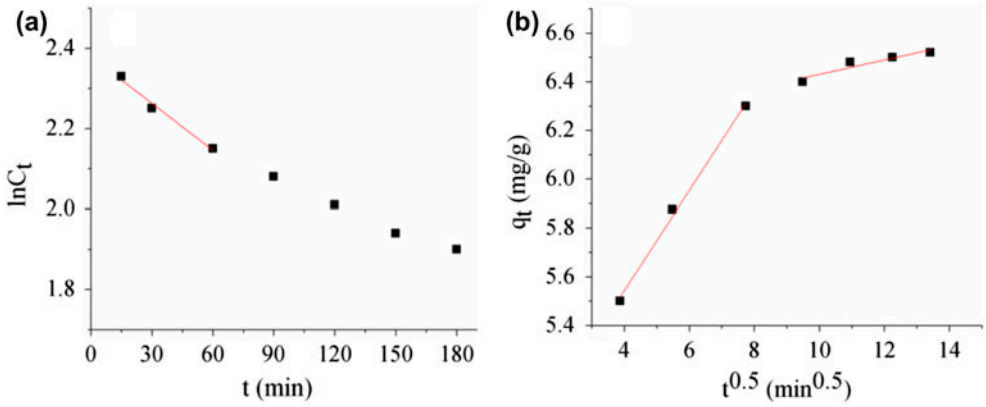

Fig. 11. Spahn and Schlunder model (a) and Intraparticle diffusion model (b) for the adsorption of Ni(II) by NH_2-MCM-41.

Table 8
The XRF data of NH_2-MCM-41 before and after adsorption

	NH_2-MCM-41	Ni(II)-NH_2-MCM-41
SiO_2 (m/m%)	93.03	93.25
Al_2O_3 (m/m%)	5.56	4.70
NiO (m/m%)	0	0.95

4. Conclusions

RSM was used to optimize the adsorption of Ni(II) using NH_2-MCM-41. The solution pH, metal concentration, temperature, and adsorbent dosage significantly influence Ni(II) removal efficiency, while the maximum value (93.20%) was achieved at 6.50, 10.00 mg/L, 35°C, and 5.00 g/L, respectively. Langmuir model depicted the experiment data better and the maximum adsorption capacity was 14.34 mg/g. The kinetic data showed the adsorption of Ni(II) fitted well with pseudo-second-order model. Moreover, the intraparticle diffusion model indicated three stages of the adsorption process: fast uptake, intraparticle diffusion, and equilibrium stage. The calculated thermodynamic parameters hinted the adsorption of Ni(II) by NH_2-MCM-41 was feasible, endothermic, and spontaneous. Besides, NH_2-MCM-41 can be a potential adsorbent for Ni(II).

References

[1] R. Singhon, J. Husson, M. Knorr, B. Lakard, M. Euvrard, Adsorption of Ni(II) ions on colloidal hybrid organic–inorganic silica composites, Colloids Surf., B 93 (2012) 1–7.
[2] C. Borba, R. Guirardello, E. Silva, M. Veit, C. Tavares, Removal of nickel(II) ions from aqueous solution by biosorption in a fixed bed column: Experimental and theoretical breakthrough curves, Biochem. Eng. J. 30 (2006) 184–191.
[3] E. Malkoc, Y. Nuhoglu, Removal of Ni(II) ions from aqueous solutions using waste of tea factory: Adsorption on a fixed-bed column, J. Hazard. Mater. 135 (2006) 328–336.
[4] L. Li, F. Liu, X. Jing, P. Ling, A. Li, Displacement mechanism of binary competitive adsorption for aqueous divalent metal ions onto a novel IDA-chelating resin: Isotherm and kinetic modeling, Water Res. 45 (2011) 1177–1188.
[5] M. Ahmaruzzaman, V.K. Gupta, Rice husk and its ash as low-cost adsorbents in water and wastewater treatment, Ind. Eng. Chem. Res. 50 (2011) 13589–13613.
[6] V. Mavrov, T. Erwe, C. Blöcher, H. Chmiel, Study of new integrated processes combining adsorption, membrane separation and flotation for heavy metal removal from wastewater, Desalination 157 (2003) 97–104.
[7] X. Gu, L.J. Evans, Surface complexation modelling of Cd(II), Cu(II), Ni(II), Pb(II) and Zn(II) adsorption onto kaolinite, Geochim. Cosmochim. Acta 72 (2008) 267–276.
[8] M. Kobya, E. Demirbas, E. Senturk, M. Ince, Adsorption of heavy metal ions from aqueous solutions by activated carbon prepared from apricot stone, Bioresour. Technol. 96 (2005) 1518–1521.
[9] E. Malkoc, Y. Nuhoglu, Investigations of nickel(II) removal from aqueous solutions using tea factory waste, J. Hazard. Mater. 127 (2005) 120–128.
[10] M.N. Zafar, R. Nadeem, M.A. Hanif, Biosorption of nickel from protonated rice bran, J. Hazard. Mater. 143 (2007) 478–485.
[11] S.A. Idris, C.M. Davidson, C. McManamon, M.A. Morris, P. Anderson, L.T. Gibson, Large pore diameter MCM-41 and its application for lead removal from aqueous media, J. Hazard. Mater. 185 (2011) 898–904.
[12] S. Jabariyan, M.A. Zanjanchi, A simple and fast sonication procedure to remove surfactant templates from mesoporous MCM-41, Ultrason. Sonochem. 19 (2012) 1087–1093.
[13] A. Hokura, I. Nakai, H. Yamada, Primary study on capturing behavior for transition metal ions on mesoporous silicate (MCM-41), J. Ion Exch. 14 (2003) 173–176.
[14] K. Parida, S.K. Dash, Adsorption of Cu^{2+} on spherical Fe-MCM-41 and its application for oxidation of adamantane, J. Hazard. Mater. 179 (2010) 642–649.

[15] Q. Qin, J. Ma, K. Liu, Adsorption of anionic dyes on ammonium-functionalized MCM-41, J. Hazard. Mater. 162 (2009) 133–139.
[16] A. Witek-Krowiak, K. Chojnacka, D. Podstawczyk, A. Dawiec, K. Pokomeda, Application of response surface methodology and artificial neural network methods in modelling and optimization of biosorption process, Bioresour. Technol. 160 (2014) 150–160.
[17] M. Jain, V. Garg, K. Kadirvelu, Investigation of Cr(VI) adsorption onto chemically treated *Helianthus annuus*: Optimization using response surface methodology, Bioresour. Technol. 102 (2011) 600–605.
[18] Y. Wu, Y. Jin, J. Cao, P. Yilihan, Y. Wen, J. Zhou, Optimizing adsorption of arsenic(III) by NH_2-MCM-41 using response surface methodology, J. Ind. Eng. Chem. 20 (2013) 2792–2800.
[19] P. Faria, J. Órfão, M. Pereira, Adsorption of anionic and cationic dyes on activated carbons with different surface chemistries, Water Res. 38 (2004) 2043–2052.
[20] H. Yoshitake, T. Yokoi, T. Tatsumi, Adsorption of chromate and arsenate by amino-functionalized MCM-41 and SBA-1, Chem. Mater. 14 (2002) 4603–4610.
[21] V.M. Boddu, K. Abburi, J.L. Talbott, E.D. Smith, R. Haasch, Removal of arsenic (III) and arsenic (V) from aqueous medium using chitosan-coated biosorbent, Water Res. 42 (2008) 633–642.
[22] P.X. Sheng, Y.P. Ting, J.P. Chen, L. Hong, Sorption of lead, copper, cadmium, zinc, and nickel by marine algal biomass: Characterization of biosorptive capacity and investigation of mechanisms, J. Colloid Interface Sci. 275 (2004) 131–141.
[23] X. Sun, B. Peng, Y. Ji, J. Chen, D. Li, Chitosan(chitin)/cellulose composite biosorbents prepared using ionic liquid for heavy metal ions adsorption, AlChE J. 55 (2009) 2062–2069.
[24] A.M. Vargas, A.C. Martins, V.C. Almeida, Ternary adsorption of acid dyes onto activated carbon from flamboyant pods (*Delonix regia*): Analysis by derivative spectrophotometry and response surface methodology, Chem. Eng. J. 195-196 (2012) 173–179.
[25] Z. Wu, H. Li, J. Ming, G. Zhao, Optimization of adsorption of tea polyphenols into oat β-glucan using response surface methodology, J. Agric. Food. Chem. 59 (2010) 378–385.
[26] S. Yang, G. Sheng, X. Tan, J. Hu, J. Du, G. Montavon, X. Wang, Determination of Ni(II) uptake mechanisms on mordenite surfaces: A combined macroscopic and microscopic approach, Geochim. Cosmochim. Acta 75 (2011) 6520–6534.
[27] S. Yang, J. Li, Y. Lu, Y. Chen, X. Wang, Sorption of Ni (II) on GMZ bentonite: Effects of pH, ionic strength, foreign ions, humic acid and temperature, Appl. Radiat. Isot. 67 (2009) 1600–1608.
[28] H. Genç-Fuhrman, J.C. Tjell, D. McConchie, Adsorption of arsenic from water using activated neutralized red mud, Environ. Sci. Technol. 38 (2004) 2428–2434.
[29] B. Hameed, Spent tea leaves: A new non-conventional and low-cost adsorbent for removal of basic dye from aqueous solutions, J. Hazard. Mater. 161 (2009) 753–759.
[30] I. Langmuir, The adsorption of gases on plane surfaces of glass, mica and platinum, J. Am. Chem. Soc. 40 (1918) 1361–1403.
[31] H. Freundlich, Über die adsorption in lösungen (Over the adsorption in solution), Z. Physik. Chem 57 (1907) 385–470.
[32] M. Dubinin, L. Radushkevich, Equation of the characteristic curve of activated charcoal, Chem. Zentralbl. 1 (1947) 875.
[33] A. Sari, M. Tuzen, D. Citak, M. Soylak, Equilibrium, kinetic and thermodynamic studies of adsorption of Pb(II) from aqueous solution onto Turkish kaolinite clay, J. Hazard. Mater. 149 (2007) 283–291.
[34] Y. Ho, J. Porter, G. McKay, Equilibrium isotherm studies for the sorption of divalent metal ions onto peat: Copper, nickel and lead single component systems, Water Air Soil Pollut. 141 (2002) 1–33.
[35] M.S. Onyango, Y. Kojima, A. Kumar, D. Kuchar, M. Kubota, H. Matsuda, Uptake of fluoride by Al^{3+} pretreated low-silica synthetic zeolites: Adsorption equilibrium and rate studies, Sep. Sci. Technol. 41 (2006) 683–704.
[36] K. Krishnani, X. Meng, L. Dupont, Metal ions binding onto lignocellulosic biosorbent, J. Environ. Sci. Health. Part A Toxic/Hazard. Subst. Environ. Eng. 44 (2009) 688–699.
[37] K.K. Krishnani, X. Meng, C. Christodoulatos, V.M. Boddu, Biosorption mechanism of nine different heavy metals onto biomatrix from rice husk, J. Hazard. Mater. 153 (2008) 1222–1234.
[38] R. Coşkun, C. Soykan, M. Saçak, Adsorption of copper(II), nickel(II) and cobalt(II) ions from aqueous solution by methacrylic acid/acrylamide monomer mixture grafted poly (ethylene terephthalate) fiber, Sep. Purif. Technol. 49 (2006) 107–114.
[39] Z. Zeledón Toruño, C. Lao Luque, M. Solé Sardans, Nickel and copper removal from aqueous solution by an immature coal (leonardite): Effect of pH, contact time and water hardness, J. Chem. Technol. Biotechnol. 80 (2005) 649–656.
[40] L. Cui, G. Wu, T.s. Jeong, Adsorption performance of nickel and cadmium ions onto brewer's yeast, Can. J. Chem. Eng. 88 (2010) 109–115.
[41] K.A. Northcott, K. Miyakawa, S. Oshima, Y. Komatsu, J.M. Perera, G.W. Stevens, The adsorption of divalent metal cations on mesoporous silicate MCM-41, Chem. Eng. J. 157 (2010) 25–28.
[42] G. Schüürmann, First-order and pseudo-first-order elimination kinetics, Sci. Total Environ. 109–110 (1991) 395–405.
[43] Y.S. Ho, G. McKay, Pseudo-second order model for sorption processes, Process Biochem. 34 (1999) 451–465.
[44] Y.S. Ho, G. McKay, The kinetics of sorption of divalent metal ions onto sphagnum moss peat, Water Res. 34 (2000) 735–742.
[45] W. Fritz, W. Merk, E. Schlünder, Competitative adsorption of two dissolved organics onto activated carbon—II, Chem. Eng. Sci. 36 (1981) 743–757.
[46] G. Panda, S. Das, T. Bandopadhyay, A. Guha, Adsorption of nickel on husk of *Lathyrus sativus*: Behavior and binding mechanism, Colloids Surf., B 57 (2007) 135–142.
[47] F.C. Wu, R.L. Tseng, R.S. Juang, Kinetic modeling of liquid-phase adsorption of reactive dyes and metal ions on chitosan, Water Res. 35 (2001) 613–618.